J. Fluid Mech. (2006), *vol.* 567, *pp.* 379–397.
doi:10.1017/S0022112006002382 Printed in the United Kingdom

Steady axisymmetric creeping plumes above a planar boundary. Part 2. A distributed source

By ROBERT J. WHITTAKER AND JOHN R. LISTER

Institute of Theoretical Geophysics, Department of Applied Mathematics and Theoretical Physics, University of Cambridge, Wilberforce Road, Cambridge, CB3 0WA, UK

(Received 1 September 2005 and in revised form 10 May 2006)

Asymptotic solutions are obtained for an axisymmetric plume rising from a localized heat source at the base of a half-space filled with very viscous fluid. Specifically, we consider sources comprising a heated disk with either rigid (no-slip) or free-slip (no tangential stress) conditions on the lower boundary. The boundary layer which forms above the source is solved using stretched coordinates, and then matched to a slender plume which rises above it. At large Rayleigh numbers, the Nusselt number is given by $Nu \sim 4.06Ra^{1/3}(\ln Ra)^{-1/3}$ (free-slip boundary) and $Nu \sim 2.90Ra^{1/5}$ (rigid boundary), where the Rayleigh number is based on the radius of the source. Both these expressions have corrections arising from a slender-body expansion in powers of $(\ln Ra)^{-1}$.

1. Introduction

In Part 1 of this work (Whittaker & Lister 2006), we derived an asymptotic solution for a slender plume in Stokes flow above a horizontal boundary due to a point source of given buoyancy flux B. This was found to depend only on B, the properties of the fluid, and the boundary condition on the velocity at the boundary. Actual realizations of this flow will involve a buoyancy source of finite size. If the source is fixed temperature, rather than fixed flux, then B will also need to be determined by a solution in the neighbourhood of the source. In this paper, we address the question of how to do this when the source is not point-like.

For a source of typical linear dimension R, held at constant temperature $T_0 + \Delta T$, with a far-field temperature T_0, we define the Rayleigh and Nusselt numbers by

$$Ra = \frac{g\beta\Delta T\, R^3}{\nu\kappa}, \qquad Nu = \frac{B}{g\beta\Delta T\,\kappa R}, \tag{1.1}$$

where g is the acceleration due to gravity, and β, κ and ν are, respectively, the coefficients of thermal expansion, thermal diffusivity and kinematic viscosity of the fluid. Then Ra and Nu are the usual dimensionless measures of the thermal forcing and the resulting heat flux. We note that the length scale $z_0 = 4\kappa(2\pi\nu/B)^{1/2}$ introduced in Part 1, can be expressed as

$$z_0/R = C\,(RaNu)^{-1/2}, \tag{1.2}$$

where $C = (32\pi)^{1/2}$.

If $Ra \ll 1$, then the solution to the heat equation on the length scale R of the source is dominated by diffusion. Then $Nu = O(1)$ and $z_0 \gg R$. The effects of advection become comparable to those of diffusion on the length scale z_0. This is the scale on

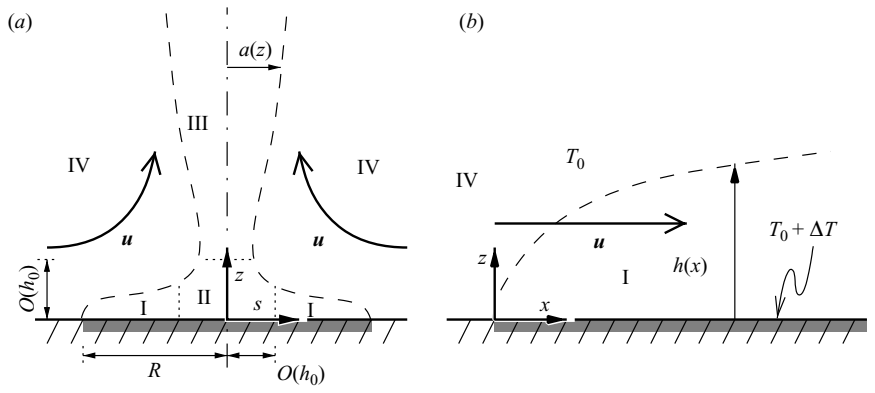

FIGURE 1. (*a*) An overview of the different regions of the flow, showing the horizontal boundary layer I, the turn-round region II, the vertical plume III, and the outer flow IV. The scale h_0 of the turn-round region is much smaller than the radius R of the disk, and matches the boundary-layer thickness H for $s \ll z$ to the plume radius a for $z \ll R$. (*b*) A close-up of the horizontal boundary layer, with horizontal coordinate $x = R - s$ centred on the outer edge.

which the local Rayleigh number is $O(1)$, and also where the plume radius a becomes comparable to the rise height z. The point-source solution derived in Part 1 is valid for $z \gg z_0$ (equivalently $a \ll z$). In this situation, B is determined by diffusion on the length scale R and the source appears point-like on the much larger scale z_0 of the plume base (cf. flow past a heated body at low Péclet number; Leal 1992, pp. 456 ff).

If $Ra \gg 1$ then we expect the solution close to the source (on the length scale R) to involve boundary layers in which both advection and diffusion are important. Motivated by experimental realizations (for example, Kaminski & Jaupart 2003; Kerr & Mériaux 2004), we consider the specific case of a source that is a heated disk of radius R set into the horizontal lower boundary. We look for a solution that takes the form shown in figure 1: radially inward flow in a boundary layer above the source (region I) feeds a central plume (region III) through a small turn-round region (region II). We find that B is determined by the competition between vertical diffusion and horizontal advection in the boundary layer. Diffusion is negligible in the turn-round region owing to the dominance of advection over the short time scale required to pass through the region. In the plume, there is a balance between advection and horizontal diffusion, allowing it to broaden slowly, but only over a height scale much greater than R.

This structure resembles part of the convection cell analysed by Umemura & Busse (1989), though we note that in their problem the boundary-layer velocity is dominated by the flow induced by the annular down-welling around the perimeter of the cell. In the present problem there is no down-welling and the flow in the boundary layer is due partly to entrainment by the rising plume, and partly to the direct action of buoyancy on the sloping isopycnals in the boundary layer. We will show that above a free-slip boundary the flow in the boundary layer is dominated by that generated by the rising plume, whereas above a rigid boundary the flow is dominated by that due to the local buoyancy forces. In both cases, we must solve an advection–diffusion problem for the temperature field in the boundary layer in order to compute the buoyancy flux released from the source. In particular, we are interested in finding the asymptotic relationship between the Nusselt number and the Rayleigh number as $Ra \to \infty$.

This problem is essentially the axisymmetric version of a two-dimensional planar problem studied by Roberts (1977). However, as in Part 1, the change from planar to axisymmetric geometry introduces logarithmic behaviour in the inner–outer flow matching, which both changes and complicates the solution. This is discussed further in § 5.3. Olson, Schubert & Anderson (1993) provided an idealized model for the axisymmetric free-slip case that we consider here. Our analysis avoids their approximations and we obtain a more accurate solution. The simplifying assumptions made by Olson *et al.* (1993) can be seen from our analysis to be reasonable, though not strictly true. As a result, their approximate scaling $Nu \propto Ra^{1/3}$ compares favourably with the correct leading-order result $Nu \sim 4.06\, Ra^{1/3}(\ln Ra)^{-1/3}$ that we derive for the free-slip problem.† We also derive the scaling $Nu \sim 2.90\, Ra^{1/5}$ for the case of a rigid boundary. The lack of a logarithmic factor in the rigid case is a reflection of the fact that the boundary-layer flow is not influenced by the plume at leading order.

1.1. *Notation and governing equations*

As in Part 1, the governing equations we consider are the Boussinesq Stokes equations for incompressible flow, and the steady advection–diffusion equation for heat. We write

$$\nu \nabla^2 \boldsymbol{u} = \nabla p - b\hat{\boldsymbol{e}}_z, \tag{1.3}$$

$$\nabla \cdot \boldsymbol{u} = 0, \tag{1.4}$$

$$(\boldsymbol{u} \cdot \nabla)\, b = \kappa \nabla^2 b, \tag{1.5}$$

where $b = g\beta(T - T_0)$ denotes the buoyancy distribution, p is a modified pressure and the remaining notation is standard.

The boundary conditions are a quiescent far field with $b \to 0$, a velocity condition (either rigid or free-slip) on the lower boundary $z = 0$, and appropriate thermal conditions on $z = 0$: $b = g\beta\Delta T$ for $s < R$, and $b_z = 0$ for $s > R$. We generally use cylindrical polar coordinates (s, ϕ, z), as shown in figure 1, and we consider only the axisymmetric case, in which all variables are independent of ϕ.

2. Structure of the plume

2.1. *Plume width and mass flux*

The turn-round region (region II of figure 1*a*) is defined by the region in which horizontal and vertical derivatives have the same order of magnitude, in other words where the slope of the streamlines is roughly $O(1)$. Once the heated fluid has risen out of the turn-round region, the plume width $a(z)$ satisfies $a \ll z$ and the plume is slender. As in Part 1, vertical diffusion can be neglected, with $O(a^2/z^2)$ corrections, and the buoyancy flux

$$B = 2\pi \int_0^\infty wb\, s \, \mathrm{d}s, \tag{2.1}$$

is constant. Moreover, slenderness implies that the vertical velocity is uniform across the plume at leading order with $O([\ln(z/a)]^{-1})$ corrections. The Stokes stream-function therefore takes the form $\psi \sim s^2 w_0(z)/2$ at leading order. The horizontally integrated buoyancy force is given by

$$F(z) = 2\pi \int_0^\infty bs \, \mathrm{d}s \sim \frac{B}{w_0(z)}. \tag{2.2}$$

† After seeing a conference presentation of our work Professor S. Morris kindly sent us an unpublished manuscript from 1987, in which he also derived this leading-order result.

We use a ratio of two moments of the buoyancy distribution $b(s, z)$ to define a representative (thermal) width of the plume as

$$a^2 = \frac{\int_0^\infty b\, s^3 \,\mathrm{d}s}{\int_0^\infty b\, s \,\mathrm{d}s}. \tag{2.3}$$

With this definition, the width of a Gaussian distribution $b \propto \exp[-(s/a)^2]$ (see Part 1) is precisely a. We then define a representative mass flux in the plume by

$$Q(z) = \frac{2\int_0^\infty b\, \psi \,\mathrm{d}\psi}{\int_0^\infty b \,\mathrm{d}\psi}, \tag{2.4}$$

where the factor of 2 is introduced so that $Q(z) = a^2 w_0$ in uniform flow. We define Q in terms of ψ as this definition may also be applied to non-uniform flow. In particular, it will be used later for matching the flow in the boundary layer to the base of the plume.

Since Q depends on the width of the buoyancy distribution, it increases along the flow owing to the diffusion of heat across streamlines. This effect is now quantified. Using ψ as the horizontal coordinate and neglecting vertical diffusion, the heat equation (1.5) may be rewritten as

$$\left(\frac{\partial b}{\partial z}\right)_\psi = 2\kappa \frac{\partial}{\partial \psi}\left(\psi \frac{\partial b}{\partial \psi}\right). \tag{2.5}$$

It follows from (2.5) that

$$\frac{\mathrm{d}}{\mathrm{d}z}\int_0^\infty b \,\mathrm{d}\psi = 0, \tag{2.6}$$

reflecting the constancy of B, and that

$$\frac{\mathrm{d}}{\mathrm{d}z}\int_0^\infty b\psi \,\mathrm{d}\psi = [2\kappa\psi^2 b_\psi]_0^\infty - 2\kappa\int_0^\infty b_\psi \psi \,\mathrm{d}\psi = 2\kappa\int_0^\infty b \,\mathrm{d}\psi. \tag{2.7}$$

Hence $\mathrm{d}Q/\mathrm{d}z = 4\kappa$, and so

$$Q(z) = 4\kappa(z + z^*) \tag{2.8}$$

for some constant z^*, which can be interpreted as the depth (below the plane) of a virtual origin for the plume. (A point-source plume has $z^* = 0$.) In the present problem, z^* is set by the mass flux entering from the turn-round region at the base of the plume. For $z \ll z^*$, we observe that $Q(z) \sim 4\kappa z^*$, so there is little diffusion across the streamlines and the plume is advection dominated in this region.

After solving the appropriate boundary-layer problem, Q and B will be matched through the turn-round region, which is sufficient to determine both the leading-order behaviour of the plume and the leading-order flow that it induces in the outer fluid. Complete matching of $b(\psi)$ is discussed further in the Appendix.

2.2. *Slender-body theory for the vertical velocity*

Since $a \ll z$, slender-body theory (Cox 1970; Leal 1992, pp. 247–251) may be used to show that the leading-order vertical flow for $s \ll z$ induced by the buoyancy force

$F(z)$ is given by

$$w(s,z) = \frac{F(z)}{2\pi\nu}\left[\ln\left(\frac{z}{s}\right) + O(1)\right], \tag{2.9}$$

for both rigid and free-slip boundary conditions, as in Part 1. By matching this to the rise velocity $w_0(z)$ of the plume and using (2.2), we obtain

$$w_0^2(z) = \frac{B}{4\pi\nu}\left[\ln\left(\frac{z^2}{a^2}\right) + O(1)\right]. \tag{2.10}$$

The interior structure of the plume does not play a role at leading order.

Introducing $\epsilon = B/(2\pi\nu w_0^2)$, and using $a^2 = Q/w_0$ and (2.8), we obtain

$$\frac{2}{\epsilon} + \tfrac{1}{2}\ln\epsilon = \ln Z(z), \tag{2.11}$$

where

$$Z(z) = \frac{z^2}{z_0(z+z^*)}. \tag{2.12}$$

Solving (2.11) for $\epsilon \ll 1$, and substituting into (2.10) and (2.2), we deduce that

$$\epsilon(z) \sim \frac{2}{\ln Z(z)}\left(1 - \frac{\ln\ln Z(z)}{2\ln Z(z)}\right), \tag{2.13}$$

$$w_0(z) \sim \left(\frac{B\ln Z(z)}{4\pi\nu}\right)^{1/2}\left(1 + \frac{\ln\ln Z(z)}{4\ln Z(z)}\right), \tag{2.14}$$

$$F(z) \sim \left(\frac{4\pi\nu B}{\ln Z(z)}\right)^{1/2}\left(1 - \frac{\ln\ln Z(z)}{4\ln Z(z)}\right). \tag{2.15}$$

We note that if $z \gg z^*$ then $Z \sim z/z_0$ and expressions (2.13)–(2.15) reduce to those for the point-source plume studied in Part 1. If $z \ll z^*$ then $Z \sim z^2/(z_0 z^*)$; the base of the plume is where $z \sim a \sim (z_0 z^*)^{1/2}$ or, equivalently, $Z = O(1)$.

Given the form of $\epsilon(z)$, it is possible to compute the entire outer velocity field at leading order. The calculations are essentially the same as in Appendix B of Part 1, so we omit the details here. The calculation verifies the slender-body result (2.9), and also provides the plume-induced velocity field in the boundary layer above the source.

2.3. *Scaling arguments for the ordering of the length scales*

As seen in (2.8) and (2.12), the behaviour of the plume changes over a vertical scale comparable with the depth z^* of the virtual origin. It is therefore of interest to know the size of z^* relative to both the height h_0 of the turn-round region (for the matching there) and the size R of the source (for determining the flow induced in the boundary layer).

We are considering $Ra \gg 1$ here, and so expect that $Nu \gg 1$. The boundary layer above the source will therefore be thin compared to the size of the source, and so we expect $h_0 \ll R$. Since the velocity in the boundary layer will be smaller than that in the plume (owing to the shallow slope of the isopycnals and to the closer proximity with the boundary), the boundary layer will thicken more over a radial distance R than a point-source plume of similar buoyancy would thicken over a height R. We therefore anticipate that $z^* \gg R$, and hence also $z^* \gg h_0$. Order-of-magnitude matching at the base of the plume shows that both a and z are $O(h_0)$, and hence

$$h_0^2 = O(z_0 z^*). \tag{2.16}$$

In conclusion, we deduce that the various length scales are ordered as follows:

$$z_0 \ll h_0 \ll R \ll z^*. \tag{2.17}$$

In particular, we note that the matching between the plume and the turn-round region takes place in the lower advection-dominated ($z \ll z^*$) part of the plume, where $Q(z) \sim 4\kappa z^*$ and $Z(z) \sim z^2/(z_0 z^*)$. These results will be verified by the complete solution.

3. Solution for a free-slip boundary

We now turn to the specific case of a free-slip boundary, and start with the assumption (verified below in § 3.4) that the flow in the boundary layer is dominated by that induced by the plume. The solution strategy is then as follows.

Referring to figure 1(*a*), the outer flow (region IV) is driven by the plume (III), and in turn determines the leading-order velocity field in the boundary layer (I). Solution of an advection–diffusion problem (with the prescribed velocity field due to the plume) then gives the buoyancy field in the boundary layer. From this we can compute the mass and buoyancy fluxes entering the turn-round region (II), and thence the base of the plume. This closes the problem.

3.1. *The plume-induced flow in the boundary layer*

The plume solution of § 2 allows us to compute the velocity field close to the horizontal boundary in terms of the buoyancy flux B and the depth z^* of the virtual origin. This can be accomplished either by direct asymptotic approximation of an integral representation (see § 4.1 of Part 1), or by evaluation of the full outer velocity field from $F(z)$ (see Appendix B of Part 1). Either way, we find that the leading-order velocity for $z \ll s$ near the free-slip boundary is given by

$$\boldsymbol{u} = -u(s)\,\hat{\boldsymbol{e}}_s + \frac{z}{s}\frac{\partial}{\partial s}(s\,u(s))\hat{\boldsymbol{e}}_z, \tag{3.1}$$

where the radial inflow is given by

$$u(s) \sim \left(\frac{B}{4\pi\nu \ln Z(s)}\right)^{1/2}\left(1 - \frac{\ln\ln Z(s)}{4\ln Z(s)}\right), \tag{3.2}$$

and the function $Z(z)$ is as defined in (2.12). This represents an almost uniform radial inflow, with a small vertical velocity to respect mass conservation.

Since $h_0 \ll R$ for $Ra \gg 1$, the plug flow (3.1) describes the leading-order velocity in the thermal boundary layer up to the turn-round region, where $s = O(h_0)$ and the velocity becomes more like a stagnation-point flow.

3.2. *The buoyancy field in the boundary layer*

To solve the heat equation in the boundary layer above the source, we adopt a horizontal coordinate, $x = R - s$, centred on the outer edge of the heated region, as shown in figure 1(*b*). Using (3.1) and making the usual boundary-layer approximations, the heat equation (1.5) becomes

$$u\frac{\partial b}{\partial x} - \frac{z}{s}\frac{\partial (su)}{\partial x}\frac{\partial b}{\partial z} = \kappa\frac{\partial^2 b}{\partial z^2}, \tag{3.3}$$

where the radial inflow u is prescribed by (3.2). This is to be solved in $x, z > 0$, subject to the boundary conditions

$$b = 0 \text{ at } x = 0 \text{ and as } z \to \infty, \quad b = g\beta\Delta T \text{ on } z = 0. \tag{3.4}$$

In fact, as is well-known, it is possible to use a coordinate transformation to find a similarity solution to (3.3)–(3.4) for an arbitrary inflow $u(s)$. The buoyancy field is written as a function of a scaled vertical coordinate $z/h(x)$ and, on making this change of variables, it becomes clear how $h(x)$ should be chosen to obtain self-similarity. A simple second-order ODE is then solved to find the buoyancy distribution. We obtain

$$h(x) = \frac{2}{su}\left(\kappa \int_0^x s^2 u \,\mathrm{d}x\right)^{1/2}, \tag{3.5}$$

$$b(x, z) = g\beta\Delta T \,\mathrm{erfc}\left(\frac{z}{h(x)}\right). \tag{3.6}$$

We define the horizontal buoyancy flux

$$B_\mathrm{h}(x) = 2\pi s \int_0^\infty u(s)\, b(x, z)\,\mathrm{d}z, \tag{3.7}$$

and define a representative horizontal mass flux $Q_\mathrm{h}(x)$ using (2.4). Substituting from (3.5) and (3.6), we re-express these integrals as

$$B_\mathrm{h}(x) = 4g\beta\Delta T\left(\pi\kappa \int_0^x s^2 u \,\mathrm{d}x\right)^{1/2}, \tag{3.8}$$

$$Q_\mathrm{h}(x) = \left(\pi\kappa \int_0^x s^2 u \,\mathrm{d}x\right)^{1/2}. \tag{3.9}$$

Using (3.5) and (3.9), we can also eliminate $h(x)$ from (3.6) to give

$$b = g\beta\Delta T \,\mathrm{erfc}\left(\frac{\sqrt{\pi}\,\psi}{2Q_\mathrm{h}(x)}\right), \tag{3.10}$$

where $\psi(s, z) = sz\,u(s)$ is the leading-order Stokes stream-function.

Equations (3.5)–(3.10) allow us to compute the buoyancy distribution, the boundary-layer height, and the fluxes from the imposed velocity field (3.2). Note that $h(x)$ diverges as $x \to R$ (equivalently $s \to 0$) owing to the convergent stagnation-point flow near the axis. When $s = O(h)$ the boundary-layer approximation breaks down, and the fluid enters the turn-round region.

Although h diverges as $x \to R$, both $B_\mathrm{h}(x)$ and $Q_\mathrm{h}(x)$ tend to finite limits, which we denote B_0 and Q_0, respectively. As $x \to R$, the buoyancy distribution b is thus asymptotically a function only of the stream-function ψ (see figure 2). This shows that diffusive effects become negligible near the axis, and the flow is advection-dominated. Corrections from diffusion in the small turn-round region make a negligible contribution to the total mass and buoyancy fluxes from the source.

Substituting the plume-induced velocity (3.2) into (3.8) and (3.9), we find that the dominant contribution to the integrals comes from $s = O(R)$. We can therefore approximate $\ln Z(s)$ by $\ln Z(R)$ and make only an asymptotically small error. Evaluating the integrals, we obtain

$$B_0 \sim \kappa g\beta\Delta T R\left(\frac{64\pi R^2 B}{9\kappa^2\nu\,\ln Z(R)}\right)^{1/4}\left(1 - \frac{\ln\ln Z(R)}{8\ln Z(R)}\right), \tag{3.11}$$

$$Q_0 \sim \kappa R\left(\frac{\pi R^2 B}{36\kappa^2\nu\,\ln Z(R)}\right)^{1/4}\left(1 - \frac{\ln\ln Z(R)}{8\ln Z(R)}\right). \tag{3.12}$$

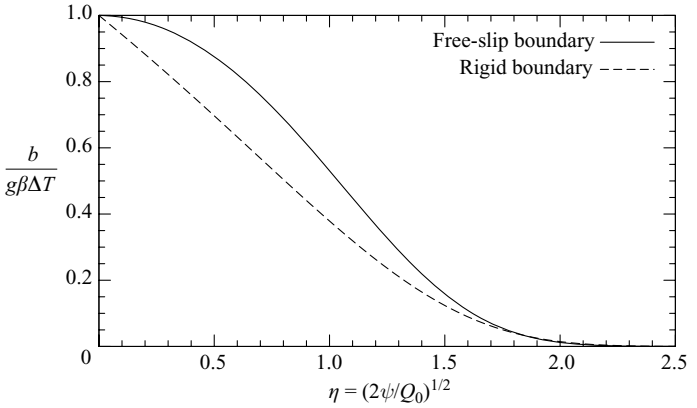

FIGURE 2. Vertical profiles of the buoyancy distribution as the fluid leaves the horizontal boundary layer and enters the turn-round region. Since the flow is advection-dominated in the turn-round region, it is natural to base the independent variable on the stream-function. The scaling is chosen so that η corresponds to the radial coordinate used in the Appendix to describe the flow in the plume. As the fluid enters the turn-round region, the vertical coordinate z is proportional to η^2 in the free-slip case, and to η in the rigid case.

3.3. *Matching the boundary layer to the plume*

The boundary layer is matched to the base of the plume via the small turn-round region near the central stagnation point. This region has a roughly $O(1)$ aspect ratio, and so a complete solution for the flow there is probably intractable analytically.

Conveniently, since diffusion is negligible in the turn-round region, $b = b(\psi)$ throughout this region, and hence the function $b(\psi)$ is known at the base of the plume from the boundary-layer solution of § 3.2. Furthermore, the leading-order outer flow driven by the plume depends only on B and z^*. These two quantities are expressible in terms of integrals of $b(\psi)$ corresponding to the buoyancy and mass fluxes, respectively. Matching through the turn-round region, we require $B = B_0$ and $z^* = Q_0/4\kappa$, where B_0 and Q_0 are given by (3.11) and (3.12), respectively. We also note that $Z(R) \sim R^2/(z_0 z^*)$ from the ordering of length scales (2.17).

Completing the matching, and rewriting the results in non-dimensional form, we obtain

$$Nu \sim \left(\frac{64\pi}{3}\right)^{1/3} Ra^{1/3} (\ln Ra)^{-1/3} \left(1 - \frac{2 \ln \ln Ra}{3 \ln Ra}\right). \tag{3.13}$$

The next correction to (3.13) is $O((\ln Ra)^{-1})$ relative to the first term, with various contributions coming from improving approximations made in the analysis.

The length scales associated with the plume are given at leading order by

$$\frac{z^*}{R} \sim \frac{1}{4}\left(\frac{\pi}{3}\right)^{1/3} Ra^{1/3} (\ln Ra)^{-1/3}, \tag{3.14}$$

$$\frac{z_0}{R} \sim (2^9 3\pi^2)^{1/6} Ra^{-2/3} (\ln Ra)^{1/6}. \tag{3.15}$$

The size of the turn-round region scales as

$$\frac{h_0}{R} = O\left(Ra^{-1/6} (\ln Ra)^{\alpha}\right), \tag{3.16}$$

where α depends on the precise definition used (e.g. $O(1)$ aspect ratio, or $O(1)$ slope of streamlines), while the typical height of the boundary layer (away from the outer edge and the divergence at the axis) scales as

$$\frac{h}{R} = O\left(Ra^{-1/3}(\ln Ra)^{1/3}\right) \sim Nu^{-1}. \tag{3.17}$$

Equations (3.14)–(3.16) confirm the ordering $z_0 \ll h_0 \ll R \ll z^*$ suggested by the scaling arguments in § 2.3.

Finally, we note that knowledge of the detailed flow $\psi(s, z)$ in the turn-round region is not necessary to complete the matching, or to calculate the internal plume structure at leading order. As shown in the Appendix, the leading-order internal structure can be determined from $b(\psi)$ at the plume base, which we know from (3.10).

3.4. *Checking the velocity in the boundary layer*

It remains to check that, within the horizontal boundary layer, the flow u_p due to the plume does indeed dominate the flow $\hat{u}$ driven by the local buoyancy forces. From (3.2), the magnitude of the horizontal flow driven by the plume satisfies

$$u_p \sim \left(\frac{B}{\nu}\right)^{1/2} (\ln Ra)^{-1/2} \sim \frac{\kappa}{R}\left(\frac{NuRa}{\ln Ra}\right)^{1/2}. \tag{3.18}$$

The typical slope of the isopycnals in the boundary layer is $O(h/R)$, leading to a horizontal pressure gradient of $O(g\beta\Delta T h/R)$. The locally driven flow is resisted by a viscous drag (from shearing of the bulk fluid) estimated as $O(\nu\hat{u}/R)$ per unit area. Balancing the driving force with the drag, we obtain

$$\hat{u} \sim \frac{\kappa h^2}{R^3} Ra \sim \frac{\kappa}{R}\frac{Ra}{Nu^2}. \tag{3.19}$$

Combining these results, we find that

$$\frac{\hat{u}}{u_p} \sim Nu^{-5/2} Ra^{1/2} (\ln Ra)^{1/2} \sim Ra^{-1/3}(\ln Ra)^{1/3} \ll 1, \tag{3.20}$$

which confirms the validity of our initial assumption.

4. Solution for a rigid boundary

Adapting the calculations of § 3 to the case of a rigid boundary, we find that the flow in the boundary layer driven by the local buoyancy forces has a greater magnitude than that driven by the rising plume: as we shall see below, the buoyancy flux arising from the locally driven flow scales as $Ra^{1/5}$, whereas the flux that results from the plume-driven flow scales as $Ra^{1/5}(\ln Ra)^{-1/5}$.

We therefore consider the horizontal boundary layer above the source in isolation, and determine the flow field and buoyancy distribution therein by solving the coupled heat and Stokes equations. From this calculation, we can find the leading-order buoyancy flux from the source, and hence the desired asymptotic relationship $Nu(Ra)$. The properties of the plume can subsequently be found by matching the mass and buoyancy fluxes as in § 3.3. However, for the rigid boundary condition, there is no feedback from the plume to the boundary layer at leading order.

4.1. *The thermal boundary layer*

Our solution for the horizontal boundary layer builds upon aspects of a number of previous studies of flow over a heated surface that use the boundary-layer

approximation (with inertia) of the Navier–Stokes equations. These studies depend on the Prandtl number $Pr = \nu/\kappa$, and our Stokes-flow problem corresponds to the limit $Pr = \infty$.

In a two-dimensional planar geometry, there is a self-similar solution for a thermal boundary layer above a semi-infinite horizontal plate held at a fixed temperature above that of the ambient fluid (Stewartson 1958; Gill, Weh & del Casal 1965). The boundary-layer thickness and horizontal velocity increase as $x^{2/5}$ and $x^{1/5}$ respectively, where x is the horizontal distance from the leading edge (see figure 1*b*). Rotem & Claassen (1969) considered the asymptotic form of this similarity solution for $Pr \gg 1$. The boundary layer is shown to split into two, and inertia is retained only in the outer layer.

In an axisymmetric geometry, the extra length scale (distance from the axis) rules out a similarity solution. For $Pr = 1$, perturbation expansions and numerical integration have been considered by Zakerullah & Ackroyd (1979) and Merkin (1983), respectively.

For the case of infinite Prandtl number considered here, there is a thin thermal boundary layer (similar to the inner layer of Rotem & Claassen 1969), which drives an outer Stokes flow with a vertical length scale R. This outer flow is purely passive, and just responds to the velocity of the thermal boundary layer below it. Since the vertical scale of the outer flow is much greater than the depth of the boundary layer (as we shall see, by a factor of $Ra^{1/5}$), the appropriate boundary condition at the upper edge of the thermal boundary layer is that the shear stress vanishes, i.e. $\partial u/\partial z \to 0$.

Introducing the Stokes stream-function ψ, and employing the usual boundary-layer approximations, we write (1.3)–(1.5) as

$$\frac{\nu}{R-x}\frac{\partial^4\psi}{\partial z^4} = \frac{\partial b}{\partial x}, \tag{4.1}$$

$$\frac{1}{R-x}\left(\frac{\partial\psi}{\partial z}\frac{\partial b}{\partial x} - \frac{\partial\psi}{\partial x}\frac{\partial b}{\partial z}\right) = \kappa\frac{\partial^2 b}{\partial z^2}\,. \tag{4.2}$$

These equations are to be solved subject to

$$\psi(x,0) = \frac{\partial\psi}{\partial z}(x,0) = 0,\ b(x,0) = g\beta\Delta T\ ; \quad \frac{\partial^2\psi}{\partial z^2}(x,\infty) = b(x,\infty) = 0\,. \tag{4.3}$$

In order to capture the singularity at the leading edge ($x = 0$), we introduce dimensionless variables

$$\bar{\xi} = \frac{x}{R}, \qquad \bar{\zeta} = \frac{z}{R}\left(\frac{x}{R}\right)^{-2/5} Ra^{-1/5}, \tag{4.4}$$

and adopt the scalings of the two-dimensional similarity solution

$$\psi = \kappa R\, Ra^{1/5}\,\bar{\xi}^{3/5}\,\bar{f}(\bar{\xi},\bar{\zeta}), \tag{4.5}$$

$$b = g\beta\Delta T\,\bar{g}(\bar{\xi},\bar{\zeta}). \tag{4.6}$$

(In the similarity solution, $\bar{f}$ and $\bar{g}$ are functions only of $\bar{\zeta}$.) Equations (4.1)–(4.3) then become

$$\frac{\partial^4\bar{f}}{\partial\bar{\zeta}^4} + (1-\bar{\xi})\left(\tfrac{2}{5}\bar{\zeta}\frac{\partial\bar{g}}{\partial\bar{\zeta}} - \bar{\xi}\frac{\partial\bar{g}}{\partial\bar{\xi}}\right) = 0, \tag{4.7}$$

$$(1-\bar{\xi})\frac{\partial^2\bar{g}}{\partial\bar{\zeta}^2} + \tfrac{3}{5}\bar{f}\frac{\partial\bar{g}}{\partial\bar{\zeta}} - \bar{\xi}\left(\frac{\partial\bar{f}}{\partial\bar{\zeta}}\frac{\partial\bar{g}}{\partial\bar{\xi}} - \frac{\partial\bar{f}}{\partial\bar{\xi}}\frac{\partial\bar{g}}{\partial\bar{\zeta}}\right) = 0, \tag{4.8}$$

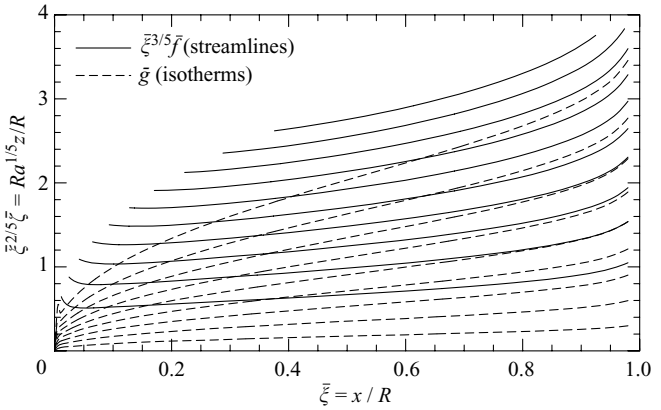

FIGURE 3. Numerical solution to (4.7)–(4.9) for the locally driven thermal boundary layer above an isothermal heated disk with a rigid boundary condition. The streamlines and isotherms are displayed at equally spaced intervals of 0.15 and 0.1, respectively.

subject to

$$\bar{f}(\bar{\xi},0) = \frac{\partial \bar{f}}{\partial \bar{\zeta}}(\bar{\xi},0) = 0, \quad \bar{g}(\bar{\xi},0) = 1, \quad \frac{\partial^2 \bar{f}}{\partial \bar{\zeta}^2}(\bar{\xi},\infty) = \bar{g}(\bar{\xi},\infty) = 0. \tag{4.9}$$

As $\bar{\xi} \to 0$, $\bar{f}$ and $\bar{g}$ can be expanded as series in $\bar{\xi}$, thus

$$\bar{f}(\bar{\xi},\bar{\zeta}) = \bar{f}_0(\bar{\zeta}) + \bar{\xi}\,\bar{f}_1(\bar{\zeta}) + O(\bar{\xi}^2), \tag{4.10}$$

$$\bar{g}(\bar{\xi},\bar{\zeta}) = \bar{g}_0(\bar{\zeta}) + \bar{\xi}\,\bar{g}_1(\bar{\zeta}) + O(\bar{\xi}^2). \tag{4.11}$$

The functions $\bar{f}_0$ and $\bar{g}_0$ are simply given by the two-dimensional similarity solution, as might be expected for an expansion about the leading edge. The higher-order terms can be calculated as regular perturbations.

4.2. *Numerical solution for the boundary layer*

In the absence of an analytic solution, the system (4.7)–(4.9) is solved numerically. The integration is accomplished by marching forwards in $\bar{\xi}$, starting from the profiles (4.10) and (4.11) at $\bar{\xi} = 0$. At each step in $\bar{\xi}$, an under-relaxed iterative technique is employed: finite-difference approximations to (4.8) and (4.7) are used to update $\bar{g}$ and $\bar{f}$ in turn, and this process is repeated until convergence is achieved for that step.

Results from the numerical calculations are shown in figure 3. The behaviour near $\bar{\xi} = 0$ matches the formal series expansion (4.10) and (4.11), while the behaviour near $\bar{\xi} = 1$ is consistent with an asymptotic prediction that the stream-function and buoyancy distribution should both tend towards functions of $\bar{\zeta}[\ln(1-\bar{\xi})]^{-1/4}$. (The latter shows the breakdown of the boundary-layer approximations as the turn-round region is approached.) The final temperature profile as $\bar{\xi} \to 1$ (i.e. as the fluid enters the turn-round region) is shown in figure 2 (dashed line).

The total heat flux from the source is computed by integrating the temperature gradient over the lower boundary:

$$B_0 = -2\pi\kappa \int_0^R \left.\frac{\partial b}{\partial z}\right|_{z=0} s\,\mathrm{d}s. \tag{4.12}$$

Rewriting this expression in terms of the variables (4.4)–(4.6), we obtain

$$Nu \sim 2\pi Ra^{1/5} \int_0^1 \left(-\frac{\partial \bar{g}}{\partial \bar{\zeta}}(\bar{\xi}, 0) \right) \frac{(1-\bar{\xi})}{\bar{\xi}^{2/5}} \, \mathrm{d}\bar{\xi}. \tag{4.13}$$

(For numerical ease, the $\bar{\xi}^{-2/5}$ singularity at the leading edge, which is identical to that in the two-dimensional case, is subtracted out and computed analytically.) From the numerical evaluation of (4.13), we obtain

$$Nu \sim 2.90\, Ra^{1/5}. \tag{4.14}$$

Similarly, using the definition (2.4), we compute the representative mass flux Q_0 from the limit as $\bar{\xi} \to 1$, to obtain

$$Q_0 \sim 0.956\, \kappa R\, Ra^{1/5}. \tag{4.15}$$

Finally, we note that the size of the turn-round region near the axis is given by

$$\frac{h_0}{R} = O(Ra^{-1/5} (\ln Ra)^{\alpha}), \tag{4.16}$$

where, as in (3.16) for the free-slip case, the exponent α depends on the precise definition used for the turn-round region.

The results (4.14) and (4.15) are the leading-order asymptotic terms as $Ra \to \infty$ from the boundary-layer solution. There are algebraically small corrections in Ra from the outer edge ($\bar{\xi} \approx 0$) and central region ($\bar{\xi} \approx 1$) of the boundary layer, where the boundary-layer approximations break down, and also logarithmically small corrections from the additional flow driven by the rising plume.

4.3. *Matching the boundary layer to the plume*

The properties of the plume are determined by matching the buoyancy and mass fluxes through the turn-round region, as in § 3.3. The fluxes from the boundary-layer are given by (4.14) and (4.15). The buoyancy flux B in the plume is simply the flux B_0 emitted by the source, and the Nusselt number is given by (4.14). Matching (4.15) with $Q(0) = 4\kappa z^*$, we find that

$$\frac{z^*}{R} \sim 0.239\, Ra^{1/5}, \tag{4.17}$$

and, using the definition (1.2) of z_0, we obtain

$$\frac{z_0}{R} \sim 5.89\, Ra^{-3/5}. \tag{4.18}$$

We note that the scalings (4.16)–(4.18) are again consistent with the ordering of length scales anticipated in § 2.3.

Finally, we check the consistency of neglecting the effects of the plume on the boundary layer and vice versa. Away from the plume and the lower boundary, the outer flow u_p driven by the plume scales as $(B/\nu)^{1/2}\, [\ln Z(r)]^{-1/2}$ (see equations (B 20) and (B 17) of Part 1, together with (2.15)). However, the effect of the no-slip boundary condition is to reduce the velocity scale by a factor of z/s for $z \ll s$. Therefore, within the boundary layer, the typical vertical shear in the radial flow driven by the plume scales like

$$\gamma_p \sim \frac{\kappa}{R^2} \left(\frac{Nu\, Ra}{\ln Ra} \right)^{1/2}. \tag{4.19}$$

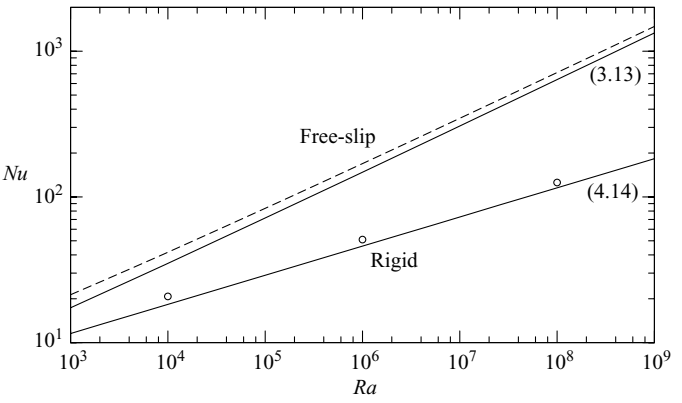

FIGURE 4. The variation of Nu with Ra for free-slip and rigid boundary conditions. The leading-order asymptotic expressions (3.13) and (4.14) are shown by the solid lines. An impression of the magnitude of the logarithmic correction terms is provided by omitting the $\ln(\ln Ra)$ term from (3.13) (dashed) and by numerical solution of the boundary-layer equation (4.2) with the plume-induced velocity added to the locally driven flow (circles). The differences from (3.13) and (4.14) are about 13 % and 10 %, respectively, at $Ra = 10^6$.

Balancing the viscous shear with the pressure gradient, we find (consistent with the scalings of § 4.1) that the locally driven shear in the boundary layer scales as

$$\bar{\gamma} \sim \frac{\kappa h^2}{R^4} Ra \sim \frac{\kappa}{R^2} \frac{Ra}{Nu^2}. \tag{4.20}$$

We combine these results to obtain

$$\frac{\bar{\gamma}}{\gamma_p} \sim Nu^{-5/2} Ra^{1/2} (\ln Ra)^{1/2} \sim (\ln Ra)^{1/2} \gg 1, \tag{4.21}$$

showing that it is indeed appropriate to neglect the effects of the plume when considering the boundary layer at leading order.

Since $h/R \sim Nu^{-1}$ is algebraically small in Ra, it can also be seen that, sufficiently far outside the boundary layer, the plume-driven flow u_p dominates the flow $\bar{u} \sim \bar{\gamma} h$ induced by the drag of the boundary layer. It is therefore appropriate to ignore the effects of the boundary-layer flow when employing the plume model of § 2.

5. Discussion and concluding remarks

5.1. *Summary*

In this paper we have presented analysis of the asymptotic structure of the axisymmetric plume above a circular heated region in a planar horizontal boundary at large Rayleigh number, for the cases of both a free-slip and a rigid boundary. The main results are (3.13) and (4.14) which give the relationship $Nu(Ra)$ as $Ra \to \infty$. In both cases there are logarithmic corrections (see figure 4). The heat flux in the plume is determined by the heat transferred into the radially inflowing horizontal boundary layer above the source. The nature of this boundary layer differs between the two boundary conditions: with a free-slip boundary, the flow in the layer is dominated by that driven by the rising plume; with a rigid boundary, the flow is dominated by that driven by the buoyancy in the layer itself.

Comparing (3.18)–(3.20) for free-slip case with (4.19)–(4.21) for the rigid case, we see that the difference in driving mechanism is associated with the different dependence

of $Nu(Ra)$. The rigid boundary condition reduces both the plume-driven and locally driven velocities by a factor of h/R. However, the slower velocities with the rigid condition lead to a thicker boundary layer and a correspondingly smaller Nusselt number. This makes the plume-induced velocity smaller, and the locally driven velocity larger. This effect is sufficient to change the dominant velocity in the boundary layer between the two boundary conditions.

The structure of the plume solutions presented here can be contrasted with previous work in a number of ways, which we group under two headings. Finally, we discuss the applicability of this work to experiments and plumes in the Earth's mantle.

5.2. *Plume structure above point and distributed sources*

For a point-source plume (studied in Part 1) there is a single vertical length scale z_0. In $z \lesssim z_0$ there is a local diffusion-dominated solution in the neighbourhood of the source; in $z \gg z_0$ there is a slender plume in which nearly vertical advection balances radial diffusion.

For a distributed source there are several distinct regions to the plume, distinguishable by the vertical length scales $h_0 = (z_0 z^*)^{1/2}$ and z^*. The turn-round region occupies $z \lesssim h_0$, where we cannot say much about the velocity field, though we do know the function $b(\psi)$. As z increases above h_0, the effective aspect ratio $\epsilon(z)$ of the plume becomes small, and the leading-order vertical velocity is then horizontally uniform. Conservation of buoyancy flux then enables us to compute the leading-order outer flow without requiring knowledge of the internal buoyancy distribution.

For $h_0 \ll z \ll z^*$, the plume is much wider at a given height than a plume of equal buoyancy flux from a point source would be. As a result, advection dominates diffusion, and the temperature distribution follows the streamlines at leading order. Over this range of heights, the plume radius and the centreline temperature remain approximately constant, with logarithmically small variations in the radius owing to the variation of the rise velocity. The small corrections due to diffusion are analysed in the Appendix, where it is also shown how to calculate the first-order correction to the rise velocity.

When $z = O(z^*)$, the plume radius is comparable to that of the corresponding point-source solution, and diffusive effects start to become significant. For $z \gtrsim z^*$, the eigenmode description in Appendix A of Part 1 is again appropriate, and radial diffusion balances vertical advection. For $z \gg z^*$, the zeroth eigenmode dominates so that the temperature profile is Gaussian, and the plume is then described well by the point-source solution. We note that $z^* \gg R$, where R is the length scale of the source.

5.3. *Comparison with a planar plume and an axisymmetric convection cell*

Table 1 provides a comparison of key scalings from the present study of an axisymmetric unbounded plume with the corresponding scalings for the analogous two-dimensional plume (Roberts 1977) and for the central plume of an axisymmetric convection cell with free-slip boundary conditions (Umemura & Busse 1989). Various similarities and differences are worth noting.

The most striking difference between the problems is in the z-dependence of the rise velocity w_0, which increases as $z^{1/2}$ in a planar geometry and logarithmically in an axisymmetric geometry. This can be attributed to the different responses of the outer Stokes flow to vertical sheet and line forces, respectively: in a planar geometry the vertical sheet force B/w_0 (per unit width in the third dimension) due to the plume's buoyancy is supported by shear stresses proportional to w_0/z in the outer flow on either side; in an axisymmetric geometry the vertical line force B/w_0 is supported by shear stresses proportional to w_0/s acting over a circular contour of length $2\pi s$.

	Two-dimensional planar plume (Roberts 1977)	Axisymmetric plume (present work)	Axisymmetric convection cell (Umemura & Busse 1989)
$Nu_{f\text{-}slip}$	$1.42\,Ra^{1/3}$	$4.06\left(\dfrac{Ra}{\ln Ra}\right)^{1/3}$	$f(\lambda)\,Ra^{1/3}$
Nu_{rigid}	$c\,Ra^{1/5}$	$2.90\,Ra^{1/5}$	–
$\dfrac{w_0 R}{\kappa}$	$\left(\mathscr{R}_1\dfrac{z}{R}\right)^{1/2}$	$[\mathscr{R}_1\ln(z/a)]^{1/2}$	$[\mathscr{R}_1\ln(z/a)]^{1/2}$
$\dfrac{z^*}{R}$	$Nu\,Ra^{-1/3}$	Nu	n/a
$\dfrac{a}{R}$ $[z \ll z^*]$	$\left(\dfrac{1}{\mathscr{R}_2}\dfrac{R}{z}\right)^{1/2}$	$\dfrac{1}{\left[\mathscr{R}_2\ln(\mathscr{R}_2 z^4/R^4)\right]^{1/4}}$	$\dfrac{1}{(\mathscr{R}_2\ln\mathscr{R}_2)^{1/4}}$
$\dfrac{a}{R}$ $[z \gg z^*]$	$\left(\dfrac{1}{\mathscr{R}_1}\dfrac{z}{R}\right)^{1/4}$	$\dfrac{(z/R)^{1/2}}{\left[\mathscr{R}_1\ln(\mathscr{R}_1 z^2/R^2)\right]^{1/4}}$	n/a

TABLE 1. Comparison of key leading-order scalings with those from related work, where $\mathscr{R}_1 = RaNu$ and $\mathscr{R}_2 = Ra/Nu$. In the Nusselt-number scalings for free-slip and rigid conditions, the function $f(\lambda)$ describes the dependence on the cell's aspect ratio λ, and the constant $c \approx 1.993$ was given incorrectly by Roberts (1977) as 1.948, owing to neglect of the locally driven boundary-layer flow. The rise velocity w_0, height z^* at which diffusion becomes important in the plume, and plume radius a depend only on the free-slip and rigid boundary conditions via the buoyancy flux as expressed in the Nusselt number. Note that many of the results shown have logarithmic correction terms which may not be much smaller for realistic parameter values; see, for example, (3.13) and figure 4.

The factor $(RaNu)^{1/2}$ reflects the dependence $w_0 \propto B^{1/2}$ in each case. The logarithmic divergence of the axisymmetric outer flow as $s \to 0$ introduces an additional weak dependence and coupling to the plume width a that is absent on the simple planar problem.

The difference between the planar and axisymmetric results for the z-dependence of the plume width a in both the advection-dominated ($z \ll z^*$) and diffusive ($z \gg z^*$) regions is a direct consequence of the different variation of the rise velocity together with conservation of buoyancy flux.

We observe that the rise velocity of an unbounded axisymmetric plume scales the same way as that of the central plume in an axisymmetric convection cell since both reflect the response to a buoyant line force. This produces a corresponding similarity between the plume width in the lower advection-dominated region ($z \ll z^*$) of the unbounded plume and that in the convection cell. The additional logarithmic dependence on z^4/R^4 for the plume reflects the need to consider heights $z/R \leqslant z^*/R \sim Nu \gg 1$; the convection cell is considered to have a height comparable to R, so that $z/R = O(1)$ and there is no space to observe significant dependence on z.

The Nusselt number scalings in the three problems involve the same algebraic powers of the Rayleigh number (1/3 or 1/5, depending on the boundary condition). This similarity masks differences in the way the flow in the horizontal boundary layer is driven (which determines the heat transfer) and is thus perhaps a little more surprising than it first appears. The boundary-layer flow for planar and axisymmetric plumes above a free-slip boundary is dominated in both cases by the flow induced by the plume; the logarithmic factor for the axisymmetric plume reflects the fact that the outer flow is logarithmically smaller than the plume velocity in a cylindrical geometry.

The absence of this factor for the axisymmetric convection cell despite the cylindrical geometry is because the boundary-layer flow is then driven by the encircling sheet-like descending plume, which has an essentially two-dimensional character, instead of by the rising central plume. The absence of a logarithmic factor for an axisymmetric plume above a rigid boundary, reflects the fact that the boundary-layer flow is driven locally in this case instead of by the plume.

Roberts (1977) assumed that the boundary-layer flow for a planar plume above a rigid boundary is dominated by the plume. In fact, the flow driven by the local buoyancy and that induced by the plume have the same order of magnitude and must therefore be considered together. We solved this coupled problem by modifying the method of § 4 to include a guessed plume-driven velocity component, and iterating to find consistency between the guessed plume flux B and the calculated boundary-layer flux B_0. Numerically, we find that $c = 1.993$, instead of the previously reported value of 1.948. The additional locally driven flow has a surprisingly small effect on the overall rate of heat transfer.

5.4. *Inertia and boundaries in the Earth's mantle and experiments*

There is an analogous condition to that given in § 6.3 of Part 1 for inertial effects to play a role in the far field. If inertia does not re-enter until $r \gg R$, then this requires

$$Pr \gg (RaNu)^{1/2} \, [\log(Ra/Nu)]^{-1/2} \, . \tag{5.1}$$

In the Earth's mantle, with Prandtl numbers of order 10^{20} or more, and Rayleigh numbers at most $O(10^8)$, this condition is certainly satisfied. Indeed, the finite vertical extent of the mantle will have a far greater effect on the flow than finite inertia.

For experiments intended to verify the asymptotic predictions, the condition (5.1) presents more of an issue. Ensuring that inertial effects are negligible at sufficiently large Rayleigh numbers for the leading-order asymptotic results to be reasonable approximations (or to be comparable with conditions in the mantle) restricts the choice of working fluids considerably. Nevertheless, it is the finite size of the experimental tank that is likely to be the most challenging constraint. Since the velocity outside the plume decays only logarithmically, any side boundaries are likely to have an effect on the solution proportional to an inverse logarithm of their distance from the plume. Experiments in confined regions might be better compared with theoretical analyses of convection cells, such as an adaptation of Umemura & Busse (1989) to use rigid boundary conditions.

Appendix. Expansion for the internal plume structure

To examine the internal structure of the plume, we employ a similar transformation to that in § 3 of Part 1, but use the fixed length z^* to replace some of the occurrences of the height z. Thus we write

$$\eta = s \left(\frac{w_0(z)}{4\kappa z^*} \right)^{1/2}, \qquad \zeta = \frac{z}{z^*}, \tag{A 1}$$

$$\psi = 4\kappa z^* \, f(\eta, \zeta), \qquad b = \frac{B}{2\pi} \frac{g(\eta, \zeta)}{4\kappa z^*}. \tag{A 2}$$

The governing equations (1.3) and (1.5), and the buoyancy-conservation equation (2.1) become

$$\left(\frac{1}{\eta} \frac{\partial}{\partial \eta} \eta \frac{\partial}{\partial \eta} \right) \frac{1}{\eta} \frac{\partial f}{\partial \eta} = -\epsilon g, \tag{A 3}$$

$$\frac{1}{\eta}\left(\frac{\partial f}{\partial \eta}\frac{\partial g}{\partial \zeta}-\frac{\partial f}{\partial \zeta}\frac{\partial g}{\partial \eta}\right)=\frac{1}{\eta}\frac{\partial}{\partial \eta}\left(\eta\frac{\partial g}{\partial \eta}\right), \tag{A 4}$$

$$\int_0^\infty \frac{\partial f}{\partial \eta}\, g\, \mathrm{d}\eta = 1, \tag{A 5}$$

where $\epsilon = B/(2\pi\nu w_0^2) \ll 1$ as before. The boundary conditions are that w and b are regular at $\eta = 0$, that $b \to 0$ as $\eta \to \infty$, that $w = w_0(z)$ at leading order, and that b and w match the initial profiles prescribed by the flow out of the turn-round region. For $z \gg h_0$, we apply these initial profiles at $z = 0$. It is then natural to pose a solution of the form

$$f(\eta,\zeta) = f_0(\eta,\zeta) + \epsilon f_1(\eta,\zeta) + \cdots, \tag{A 6}$$

$$g(\eta,\zeta) = g_0(\eta,\zeta) + \epsilon g_1(\eta,\zeta) + \cdots. \tag{A 7}$$

A.1. *Leading-order solution*

The leading-order component of (A 3) is

$$\left(\frac{1}{\eta}\frac{\partial}{\partial \eta}\eta\frac{\partial}{\partial \eta}\right)\frac{1}{\eta}\frac{\partial f_0}{\partial \eta}=0. \tag{A 8}$$

which has solution

$$f_0(\eta,\zeta) = \tfrac{1}{2}\eta^2, \tag{A 9}$$

where the normalization is chosen so that the corresponding vertical velocity is precisely $w_0(z)$. The leading-order component of (A 5) becomes

$$\int_0^\infty g_0\, \eta\, \mathrm{d}\eta = 1, \tag{A 10}$$

which provides a normalization for the buoyancy distribution.

At leading order, the heat equation (A 4) is simply

$$\frac{\partial g_0}{\partial \zeta} = \frac{1}{4\eta}\frac{\partial}{\partial \eta}\left(\eta\frac{\partial g_0}{\partial \eta}\right), \tag{A 11}$$

reflecting lateral diffusion and advection by the leading-order uniform flow. Identifying ζ with a time-like variable, (A 11) is simply the two-dimensional axisymmetric diffusion equation with a diffusion coefficient of 1/4.

Given the initial temperature profile at the base of the plume, we can solve (A 11) using the Green's function for an initial circular ring of heat (see, for example, Carslaw & Jaeger 1959, § 10.3). We obtain

$$g_0(\eta,\zeta) = \frac{2}{\zeta}\int_0^\infty \exp\left(-\frac{\eta^2+\eta'^2}{\zeta}\right) I_0\left(\frac{2\eta\eta'}{\zeta}\right) G_0(\eta')\,\eta'\,\mathrm{d}\eta', \tag{A 12}$$

where the initial dimensionless temperature profile $G_0(\eta) = g_0(\eta, 0)$ is given by

$$G_0(\eta) = \frac{2\pi\, 4\kappa z^*}{B}\, b(2\kappa z^*\eta^2) = \frac{b(2\kappa z^*\eta^2)}{\displaystyle\int_0^\infty b(2\kappa z^*\eta^2)\,\eta\,\mathrm{d}\eta} \tag{A 13}$$

and $b(\psi)$ describes the buoyancy distribution through the turn-round region (see figure 2). Using (A 12), we can confirm that the asymptotic series of Appendix A of Part 1 also describes the relaxation towards a Gaussian above a distributed source for $z \gg z^*$. We can also use (A 12) to verify equation (2.8) for $Q(z)$.

A.2. *First-order corrections*

The first-order correction to the Stokes equation is given by

$$\left(\frac{1}{\eta}\frac{\partial}{\partial\eta}\eta\frac{\partial}{\partial\eta}\right)\frac{1}{\eta}\frac{\partial f_1}{\partial\eta} = -g_0. \tag{A 14}$$

The solution may be written as

$$\frac{1}{\eta}\frac{\partial f_1}{\partial\eta} = \bar{A}(\zeta) - \int_1^\eta \frac{1}{\eta}\left(\int_0^\eta g_0\eta\,\mathrm{d}\eta\right)\,\mathrm{d}\eta, \tag{A 15}$$

where the function $\bar{A}(\zeta)$ is determined by matching with the outer flow (at a higher order than simple slender-body theory). For $\eta \gg 1$, we obtain the behaviour

$$\frac{w}{w_0} \sim 1 - \epsilon\ln\eta - \epsilon\left[\bar{A} + \int_1^\infty \frac{1}{\eta}\left(\int_\eta^\infty g_0\eta\,\mathrm{d}\eta\right)\mathrm{d}\eta\right]. \tag{A 16}$$

This is the outer limit of the inner vertical velocity, which must be matched with the inner limit of the outer flow. It is easily seen that the first two terms in (A 16) do indeed match the slender-body estimate (2.9) for the outer velocity and, as for a point source, these leading-order terms are independent of the detailed buoyancy distribution within the plume.

The first correction to the slender-body theory (see §4.3 of Part 1) yields the following result for the inner limit of the outer velocity:

$$\frac{w}{w_0} \sim \frac{F(z)}{2\pi\nu w_0(z)}\left(-\ln\left(\frac{s}{z}\right) + (\ln 2 - \delta) + \cdots\right), \tag{A 17}$$

where $\delta = 1/2$ for a free-slip boundary and 1 for a rigid boundary.

To complete the matching at $O(\epsilon)$, and hence determine $\bar{A}$, it is necessary to know the $O(\epsilon)$ correction to $F(z)$. From equation (4.7) of Part 1, this correction may be expressed in terms of an integral of $g_0 f_1'$, where f_1' is given by (A 15) and g_0 is given by (A 12). Given the initial profile G_0 from the boundary-layer solution, it is therefore possible to evaluate, at least numerically, the $O(\epsilon)$ correction to the vertical velocity in the plume.

REFERENCES

Carslaw, H. S. & Jaeger, J. C. 1959 *Conduction of Heat in Solids*, 2nd edn. Oxford University Press.

Cox, R. G. 1970 The motion of long slender bodies in a viscous fluid. Part 1. General theory. *J. Fluid Mech.* **44**, 791–810.

Gill, W. N., Weh, D. W. & del Casal, E. 1965 Free convection on a horizontal plate. *Z. Angew. Math. Phys.* **16**, 539–541.

Kaminski, E. & Jaupart, C. 2003 Laminar starting plumes in high-Prandtl-number fluids. *J. Fluid Mech.* **478**, 287–298.

Kerr, R. C. & Mériaux, C. 2004 Structure and dynamics of sheared mantle plumes. *Geochem. Geophys. Geosyst.* **5** (12).

Leal, L. G. 1992 *Laminar Flow and Convective Transport Processes*. Butterworth–Heinemann.

Merkin, J. H. 1983 Free convection above a heated horizontal disk. *Z. Angew. Math. Phys.* **34**, 596–608.

Olson, P., Schubert, G. & Anderson, C. 1993 Structure of axisymmetric mantle plumes. *J. Geophys. Res.* **98** (B4), 6829–6844.

Roberts, G. O. 1977 Fast viscous convection. *Geophys. Astrophys. Fluid Dyn.* **8**, 197–233.

ROTEM, Z. & CLAASSEN, L. 1969 Natural convection above unconfined horizontal surfaces. *J. Fluid Mech.* **39**, 173–192.

STEWARTSON, K. 1958 On the free convection from a horizontal plate. *Z. Angew. Math. Phys.* **9a**, 276–281.

UMEMURA, A. & BUSSE, F. H. 1989 Axisymmetric convection at large Rayleigh and infinite Prandtl number. *J. Fluid Mech.* **208**, 459–478.

WHITTAKER, R. J. & LISTER, J. R. 2006 Steady axisymmetric creeping plumes above a planar boundary. Part 1. A point source. *J. Fluid Mech.* **567**, 361–378.

ZAKERULLAH, M. & ACKROYD, J. A. D. 1979 Laminar natural convection boundary layers on horizontal disks. *Z. Angew. Math. Phys.* **30**, 427–435.